drones

MDPI

Article

Integrative Path Planning for Multi-Rotor Logistics UAVs Considering UAV Dynamics, Energy Efficiency, and Obstacle Avoidance †

Kunpeng Wu [1,‡], Juncong Lan [1,‡], Shaofeng Lu [1,*], Chaoxian Wu [2], Bingjian Liu [3] and Zenghao Lu [4]

[1] Shien-Ming Wu School of Intelligent Engineering, South China University of Technology, Guangzhou 511442, China; 202310191653@mail.scut.edu.cn (K.W.); 202420160725@mail.scut.edu.cn (J.L.)
[2] The School of Systems Science and Engineering, Sun Yat-sen University, Guangzhou 510275, China; wuchx35@mail.sysu.edu.cn
[3] The Department of Mechanical, Materials and Manufacturing Engineering, University of Nottingham Ningbo, Ningbo 315100, China; bingjian.liu@nottingham.edu.cn
[4] Fujian Zhongli Technology Co., Quanzhou 362100, China; zenghao@fjuav.cn
* Correspondence: lushaofeng@scut.edu.cn
† This paper is an extended version of our paper published in This article is a revised and expanded version of a paper entitled "Trajectory Planning for Multi-rotor UAV Based on Energy Cost Model", which was presented at the 2022 41st Chinese Control Conference (CCC), Hefei, China, 25–27 July 2022; pp. 1–6.
‡ These authors contributed equally to this work.

Abstract: Due to their high flexibility, low cost, and energy-saving advantages, applying Unmanned Aerial Vehicles (UAVs) in logistics is a promising field to achieve better social and economic benefits. Since UAVs' energy storage capacity is generally low, it is essential to reduce energy costs to improve their system's energy efficiency. In this paper, we proposed a novel trajectory planning framework to achieve the optimal trajectory with the minimum amount of energy consumption under the constraints of obstacles in a static environment. Based on UAV dynamics, we first derived the required power functions of multi-rotor UAVs in vertical and horizontal flight. To generate a feasible trajectory, we first adopted the A* algorithm to find a path and developed a safe flight corridor for the UAV to fly across by expanding the waypoints against the environment, and then proposed a time-discretization method to formulate the trajectory generation problem and solve it by the convex optimization algorithm. The optimization results in a static environment with obstacles demonstrated that the proposed method could efficiently and effectively obtain the optimal trajectory with the minimum amount of energy consumption under different allowed mission times and payloads. The framework would promote a variety of logistics UAV applications relevant to trajectory planning.

Keywords: multi-rotor UAVs; energy consumption model; trajectory planning; convex optimization

Academic Editors: Heng Shi, Jihong Zhu, Zheng Chen and Minchi Kuang

Received: 14 December 2024
Revised: 17 January 2025
Accepted: 22 January 2025
Published: 25 January 2025

Citation: Wu, K.; Lan, J.; Lu, S.; Wu, C.; Liu, B.; Lu, Z. Integrative Path Planning for Multi-Rotor Logistics UAVs Considering UAV Dynamics, Energy Efficiency, and Obstacle Avoidance. *Drones* **2025**, *9*, 93. https://doi.org/10.3390/drones9020093

1. Introduction

The advancement in flight control and artificial intelligence has enhanced the development of the Unmanned Aerial Vehicles industry and achieved the commercial transition from military to civilian applications. Over the past several years, industrial UAVs have been widely employed in wireless communication, plant protection, logistics distribution, and other fields [1–4]. Several companies, such as Amazon, DHL, and Google, have shown interest in UAV delivery and have begun developing their UAVs to deliver packages. Delivery using UAVs may be faster than with traditional vehicles, as the existing infrastructure

does not constrain UAVs. This makes UAVs suitable for last-mile package delivery and emergency response in forest fires and earthquakes.

Despite the benefits of integrating UAVs into logistics delivery, many practical challenges still prevent their broad deployment. On the one hand, environmental obstacles present hidden hazards to safe flights. On the other hand, the limited battery capacity of UAVs restricts their endurance and flight range, which can be affected by payload, speed, and weather conditions [5,6]. Therefore, understanding how energy consumed by UAVs changes with flight status while generating a feasible path is critical to realizing safe and energy-efficient UAV delivery. Most existing trajectory planning studies in logistics applications fail to consider the limited energy storage capacity of each UAV. By contrast, we focus on energy-efficient trajectory planning for UAVs, which can improve safety when performing missions, reduce costs, and improve efficiency.

Generally, a typical UAV trajectory planning contains two key stages: front-end path finding and back-end trajectory optimization [7]. Researchers have proposed various methods to find feasible paths in the path-finding stage to avoid collisions and generate smooth trajectories in back-end trajectory optimization. Path-finding methods based on sampling [8] and searching [9] have been proposed. Probabilistic Road-Map (PRM) [10] and Rapidly-exploring Random Tree (RRT) [11] are two well-known methods of the sampling-based method. The PRM method randomly samples points from configuration space and uses a local planner to connect these points to form a graph. Then, graph search methods are applied to find a feasible path. The RRT method starts with the root node and then produces a random extended tree by randomly adding leaf nodes. The path from the beginning to the target is obtained when the random tree's leaf nodes enter the target area. Some improved algorithms have been proposed based on the above two methods, such as HPO-RRT* [12] and APF-RRT* [13]. Searching-based methods discretize the space and transform path-finding into graph searching. The A* algorithm is a widely used searching-base method, which ensures finding a path with the minimum amount of cost. Methods based on A* include double-layer optimization A* [14] and improved A* [15], etc.

On the one hand, most path-finding methods build a geometric trajectory, which a UAV cannot execute directly due to its poor smoothness; on the other hand, trajectory optimization is required to parameterize the path in terms of time and to generate smooth and safe trajectories [16]. The primary objective of trajectory generation is to parameterize the initial geometric trajectory in time to guarantee the dynamic feasibility of the UAV. Mellinger et al. introduced a minimum snap trajectory planning method that represented the trajectory using multiple polynomial curves and ensured constraint satisfaction. The authors used the differential flatness characteristic of the UAV and obtained a smooth and dynamically feasible trajectory by minimizing the squared norm of a position derivative. Then, the trajectory planning problem was constructed as a quadratic program (QP) problem [17]. Similarly, Richter et al. provided a closed-form solution to solve the piecewise polynomial trajectory generation problem. They used RRT* as a front-end planner and applied the minimum snap method to generate a feasible trajectory. The authors also proposed a time allocation algorithm by adding the total time term to the objective function [18]. However, this approach must iteratively add intermediate waypoints to satisfy the security constraints.

Other methods involve extending the trajectory to a safe flight corridor (SFC). For instance, Chen used the A* algorithm directly to obtain a connected safe flight corridor and then generated a piecewise polynomial trajectory by quadratic programming [19,20]. Gao et al. adopted a sampling-based path-finding method to create a flight corridor composed of spheres with guaranteed safety. A minimum jerk polynomial trajectory method similar to that in Mellinger's work was used in Gao's paper to generate a trajectory,

and the problem was formulated as a quadratically constrained quadratic programming (QCQP) [21]. Furthermore, Gao et al. also utilized the A* approach to construct a safe flight corridor and to represent the trajectory using a Bernstein polynomial basis [16]. Tang et al. proposed a trajectory planning framework using B-splines and kinodynamic search [22]. Philipp et al. introduced a method that effectively addresses the time allocation problem while fully using the maneuverability of multiple rotors [23].

Due to the limited energy capacity of onboard batteries and the important role of the flying range of UAVs applied in logistics and wireless communication, recent studies on UAV trajectory and task planning began to take energy cost as an important factor [6,24–26]. Zhang et al. developed a uniform framework for better understanding the relationship between key factors and performance measures and the energy models. In addition, the authors reviewed, assessed, and classified different delivery UAV energy cost models and concluded that more studies are needed to enhance model precision [27]. In light of important factors such as energy consumption being ignored in logistics UAVs, Du et al. proposed to adopt a classic integrated model to minimize the total energy cost of multiple logistics UAVs during the delivery period of customized products. Some other studies have proposed a component model based on UAV dynamics which considers that the energy consumption of horizontal flight, takeoff, and landing is equivalent to that of hovering, and the effect of flight speed is ignored. Dorling et al. proposed that the energy consumed by a multi-rotor UAV varied linearly approximately with the weight of the battery and payload [5]. The authors also conducted experiments to validate the model and obtain relevant parameters. Cheng et al. directly used the original nonlinear model instead of approximating the power rate function to avoid the "energy infeasible" routes [28]. Du et al. addressed logistics UAV path planning by considering energy consumption constraints, customer time windows, and dynamic wind impacts. They proposed a novel hybrid GA-LNS algorithm to optimize UAV trajectories under static and dynamic wind conditions, improving energy efficiency and reducing delivery delays [29]. Rinaldi et al. proposed a hybrid auction-based task allocation framework for drone delivery systems, emphasizing energy optimization and operational persistency [30].

A more detailed two-component model comprises parasite and induced power in level flight. The former is essential for movement through the air, whereas the latter is required for staying aloft [31]. Stolaroff et al. established a model considering the latter two components to assess the greenhouse gas (GHG) emissions and energy use for drone-based delivery compared with delivery trucks [32]. Based on the two-component model, Liu et al. added the profile power required to overcome the propeller blades' rotating drag [33]. Zeng et al. used a similar model to minimize the propulsion energy and communication-related energy of UAVs in wireless communication networks [24]. Some researchers considered the impact of acceleration on energy consumption [34–36]. Gao et al. had further extended this model to an arbitrary 2D level flight and validated it through extensive experiments [37]. Chan et al. also conducted experiments to verify this model [38].

In the above discussion, the UAV energy consumption model is primarily applied in obstacle-free environments that are either one-dimensional or two-dimensional. Comprehensive energy consumption considerations are commonly applied for high-level routing problems in logistics UAVs and yet low-level trajectory planning is hardly found in relevant studies [28]. Most existing studies focused on minimum-energy trajectory optimization problems from the perspective of wireless communications without considering obstacles [6,24], and many studies focus more on trajectory smoothness and feasibility [19,21]. In the application of logistics, evaluating the impact of energy costs related to the payload

and mission time, is critical to the trajectory planning problem. Still, it has not been covered thoroughly, leading to an important research gap for further studies.

To specifically address the trajectory planning problem for logistics UAVs considering the important energy-cost issues, we proposed a new trajectory optimization model to concurrently consider the feasibility of trajectories and the energy cost characteristics of UAVs in a static 3D environment with obstacles. We proposed an energy model similar to those of the studies by Zeng et al. [24] and extended the study with an extra energy consumption model of vertical flight and obstacle-avoidance consideration. In addition, the derivation of the energy consumption models under the two flight modes is discussed in detail.

By combining a more accurate energy consumption model in trajectory planning in logistics UAVs, we aim to reduce energy costs while meeting the logistics mission demand on travel time and various payloads and that serve as a key constraint in upper-level task allocation optimization. An illustrative diagram of the trajectory planning framework is shown in Figure 1. We adopted UAV dynamics to derive the vertical and horizontal energy consumption model of multi-rotor UAVs, which was explicitly considered in our proposed trajectory planning framework.

This paper has the following two main contributions.

- Based on comprehensive UAV dynamics, we formulated the theoretical energy model for the energy consumption of multi-rotor logistics UAVs as a function of the UAV's payload weight and velocity in vertical and horizontal flight, and this model has been fully incorporated for the energy-efficient trajectory planning problem for UAVs.
- A time-discretization method was proposed to solve the optimal trajectory planning problem of multi-rotor UAVs in a static environment with obstacles, and the model was formulated as a quadratically constrained program problem that was solved efficiently and effectively to achieve the minimum energy cost under different logistics time and payload requirements.

The rest of this paper is organized as follows. Section 2 covers the modeling process where the UAV energy consumption model and the trajectory planning model are included. Section 3 demonstrates the case study and verifies the algorithm's effectiveness. In the end, conclusions are drawn, and future work is discussed in Section 4.

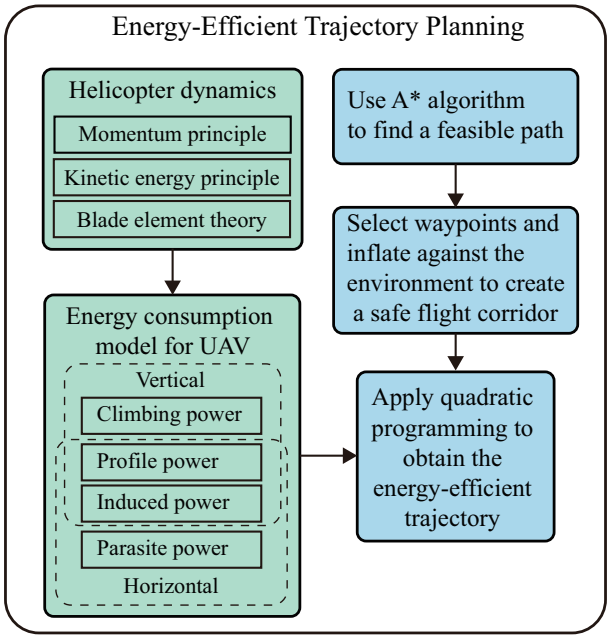

Figure 1. The proposed system diagram for logistics UAV trajectory planning.

2. Mathematical Model

In this section, we will derive the energy models of multi-rotor UAVs for both vertical and horizontal flight based on UAV dynamics [39]. Note that complicated UAV properties, such as blade flapping, are neglected. According to [40], we separately calculate the energy consumption for vertical and horizontal components. In addition, the trajectory planning problem of multi-rotor UAVs considering energy consumption during flight is initially formulated.

2.1. Energy Consumption Model of Multi-Rotor UAVs

The notations related to Section 2.1 are listed in Table 1, and the simulation values are referred in to [24].

Table 1. Notation for UAV energy model.

Notation	Description	Simulation Value
A	Rotor disc area in m^2, $A = \pi R^2$	0.503
C_D	Drag coefficient	-
D	Parasite drag in N, $D = \frac{1}{2}\rho S_{FP} V^2$	-
P_c	Climbing power (W)	-
$P_{i,v}$	Induced power of vertical flight (W)	-
$P_{i,h}$	Induced power of horizontal flight (W)	-
$P_{p,v}$	Profile power of vertical flight (W)	-
$P_{p,h}$	Profile power of horizontal flight (W)	-
P_{par}	Parasite power (W)	-
R	Rotor radius (m)	0.4
S_{FP}	Fuselage equivalent flat plate area (m^2)	0.0151
T	Thrust force (N)	-
V	Forward velocity (m/s)	-
V_c	Climbing velocity (m/s)	-
W	Weight of multi-rotor UAV (N)	20
Ω	Angular velocity of rotor (rad/s)	300
b	Number of blades	4
c	Length of chord (m)	0.0157
$\mathrm{d}D$	Drag force of blade element (N)	-
$\mathrm{d}H$	Horizontal component force of blade element (N)	-
$\mathrm{d}R$	Resultant force of blade element (N)	-
$\mathrm{d}T$	Vertical component force of blade element (N)	-
$\mathrm{d}L$	Lift force of blade element (N)	-
$\mathrm{d}r$	Width of blade element (m)	-
r	Distance from the rotation axis to the blade element (m)	-
s	Rotor solidity	0.05
$\dot{m}$	Mass flow rate (kg/s)	-
v_i	Induced velocity (m/s)	-
v_0	Induced velocity in hovering (m/s)	4.03

Table 1. *Cont.*

Notation	Description	Simulation Value
α	Angle of attack (rad)	-
ρ	Air density (kg/m^3)	1.225
σ	Average drag coefficient	0.012
κ	Incremental correction factor	0.1
μ	Advance ratio, $\mu = V/\Omega R$	-

2.1.1. Vertical Flight

We derive the induced power and climbing power using the actuator disc model. The control volume of the UAV during vertical flight can be seen in Figure 2. By applying the principles of momentum and kinetic energy, we can derive the following equations:

$$T = \dot{m}(V_c + v_{i2}) - \dot{m}V_c, \tag{1}$$

$$T(V_c + v_{i1}) = \frac{1}{2}\dot{m}(V_c + v_{i2})^2 - \frac{1}{2}\dot{m}V_c^2. \tag{2}$$

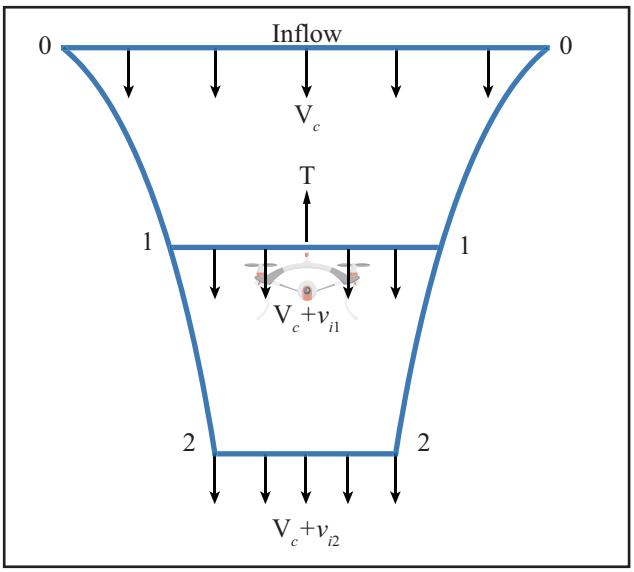

Figure 2. The control volume for vertical flight of the UAV consists of three sections. Section 0 is the upper boundary where air enters. Section 1 corresponds to the rotor disc. Section 2 is the bottom boundary where air leaves. In this context, V_c denotes the climbing velocity of the UAV, while v_{i1} and v_{i2} refer to the induced velocities in Section 1 and Section 2, respectively.

The mass flow rate of the air across the rotor disc can be represented as

$$\dot{m} = \rho A(V_c + v_{i1}), \tag{3}$$

where A represents the area of the rotor disc.

Hence, Formulas (1)–(3) can be rewritten as

$$v_{i2} = 2v_{i1}, \tag{4}$$

$$T = 2\dot{m}v_{i1} = 2\rho A(V_c + v_{i1})v_{i1}. \tag{5}$$

The Equation (4) indicates that the induced velocity v_{i1} exhibits a twofold increase in the far wake. Formula (5) establishes the quadratic relationship between induced velocity and thrust. Therefore, v_{i1} can be determined by solving (5).

$$v_{i1} = -\frac{V_c}{2} + \sqrt{\left(\frac{V_c}{2}\right)^2 + \frac{T}{2\rho A}}. \tag{6}$$

In the case of hovering flight, the induced velocity is given by

$$v_0 = \sqrt{\frac{T}{2\rho A}} = \sqrt{\frac{W}{2\rho A}}. \tag{7}$$

The climbing and induced power can be obtained by substituting (4) and (5) into (2).

$$\begin{aligned} P_c + P_{i,v} &= T(V_c + v_{i1}) \\ &= TV_c + T\left(-\frac{V_c}{2} + \sqrt{\left(\frac{V_c}{2}\right)^2 + \frac{T}{2\rho A}}\right). \end{aligned} \tag{8}$$

We use the blade element theory to derive profile power. From Figure 3, we can see the force component of an airfoil. The airfoil is subjected to profile drag opposite the direction of rotation. As can be seen from Figure 4, $\mathrm{d}D_v$ is parallel to the resultant velocity, which is generated by climbing velocity V_c, induced velocity v_i, and linear velocity Ωr. Because of $V_c + v_i \ll \Omega r$, $\mathrm{d}D_v$ can be approximately regarded as parallel to Ωr.

$$\mathrm{d}D_v = \frac{1}{2}\rho c C_D\left[(\Omega r)^2 + (V_c + v_i)^2\right]\mathrm{d}r \approx \frac{1}{2}\rho c C_D(\Omega r)^2\mathrm{d}r. \tag{9}$$

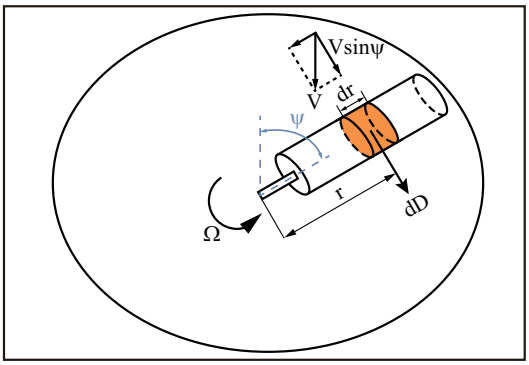

Figure 3. Illustration of velocity and forces on a rotating propeller. Ω is the angular velocity of the rotor, r is the distance from the rotation axis to the blade element, dr is the width of the blade element, and dD is the profile drag of the airfoil.

The profile power can be determined by integrating $\Omega r \mathrm{d}D_v$ from 0 to R.

$$\begin{aligned} P_{pro,v} &= b\int_0^R (\Omega r)\mathrm{d}D_v \\ &= b\int_0^R \left(\frac{1}{2}\rho c C_D(\Omega r)^2\right)(\Omega r)\mathrm{d}r \\ &= \frac{\sigma}{8}\rho b c R(\Omega R)^3 \\ &= \frac{\sigma}{8}\rho s A \Omega^3 R^3, \end{aligned} \tag{10}$$

where b is the number of blades on the propeller and $s = bcR/\pi R^2$ represents the rotor solidity. We introduce σ to denote the mean value of the profile drag coefficient.

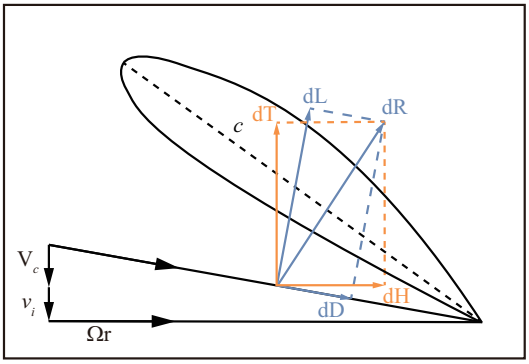

Figure 4. Illustration of force components and velocity on the airfoil. Ωr represents the airflow velocity relative to the airfoil and v_i represents the induced velocity. dL and dD denote the lift and drag forces of the airfoil, respectively, and dR is the resultant force. Additionally, dT and dH represent the vertical and horizontal components of the forces, respectively.

Therefore, the total required power for vertical flight can be expressed as

$$\begin{aligned} P_v &= P_{pro,v} + P_c + P_{i,v} \\ &= \frac{\sigma}{8}\rho s A \Omega^3 R^3 + T V_c + \\ &\kappa T\left(-\frac{V_c}{2} + \sqrt{\left(\frac{V_c}{2}\right)^2 + \frac{T}{2\rho A}}\right), \end{aligned} \tag{11}$$

where κ is a correction coefficient to account for tip losses and swirl losses [39]. Figure 5 shows the three types of power in vertical flight.

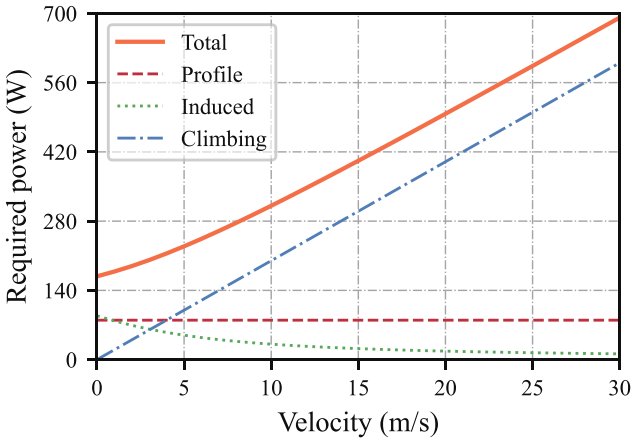

Figure 5. Profile, induced, and climbing power for vertical flight.

Since the status of the UAV when descending is related to descending speed, the vortex ring state, turbulent wake state, and windmill brake state cannot be exactly analyzed. There are no closed-form solutions for the vortex ring state and turbulent wake state. The required power is negative in the turbulent wake state and windmill brake state [39]. Accordingly, we consider $P_v = 0$ when $V_c < 0$, similar to [40].

2.1.2. Horizontal Flight

Figure 6 shows the force component of the UAV in horizontal flight at a constant velocity. We can obtain the following two equations.

$$T\cos\alpha = W, \tag{12}$$

$$T\sin\alpha = D. \tag{13}$$

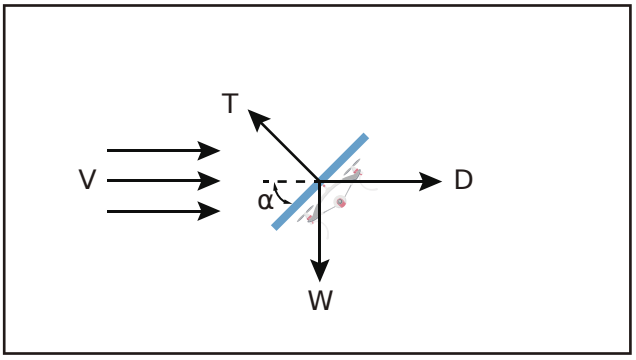

Figure 6. Schematics of the force component acting on the UAV in forward flight. α is the angle between the airflow and the rotor disc.

From Glauert's theory and substituting (13), the required power of horizontal flight can be described as

$$\begin{aligned} P_h &= P_{pro,h} + T(V\sin\alpha + v_i) \\ &= P_{pro,h} + Tv_i + DV, \end{aligned} \tag{14}$$

which includes three parts: the first is profile power, the second is induced power, and the last is parasite power.

From Figure 3, we can see that the velocity of the airfoil includes two parts in horizontal flight.

$$U_h = \Omega r + V\sin\psi, \tag{15}$$

where the first is the linear velocity and the second is the component of the forward speed.

The profile drag of the airfoil can be expressed as

$$\begin{aligned} \mathrm{d}D_h &= \frac{1}{2}\rho c C_D\left(U_h^2 + v_i^2\right)\mathrm{d}r\mathrm{d}\psi \\ &\approx \frac{1}{2}\rho c C_D(\Omega r + V\sin\psi)^2\mathrm{d}r\mathrm{d}\psi, \end{aligned} \tag{16}$$

the induced velocity is also ignored.

Hence, the profile power of horizontal flight can be expressed by integrating $U_h\mathrm{d}D_h$ from 0 to 2π and 0 to R.

$$\begin{aligned} P_{pro,h} &= \frac{b}{2\pi}\int_0^{2\pi}\int_0^R U_h\mathrm{d}D_h \\ &= \frac{b}{2\pi}\int_0^{2\pi}\int_0^R \frac{1}{2}\rho c C_D(\Omega r + V\sin\psi)^3\mathrm{d}r\mathrm{d}\psi \\ &= \frac{\sigma}{8}\rho s A\Omega^3 R^3(1+3\mu^2), \end{aligned} \tag{17}$$

where μ indicates the ratio of horizontal speed to the blade tip speed, given by $\mu = V/\Omega R$.

Figure 7 shows the actuator disc model during forward flight. Based on Glauert's formula, the relationship between thrust and induced velocity can be expressed as

$$T = (2v_i)\rho A\sqrt{(V\cos\alpha)^2 + (V\sin\alpha + v_i)^2}, \tag{18}$$

where α represents the angle between the air velocity and the rotor disc. Typically, α is small and can be regarded as 0, then $\cos\alpha$ and $\sin\alpha$ can be regarded as 1 and 0, respectively.

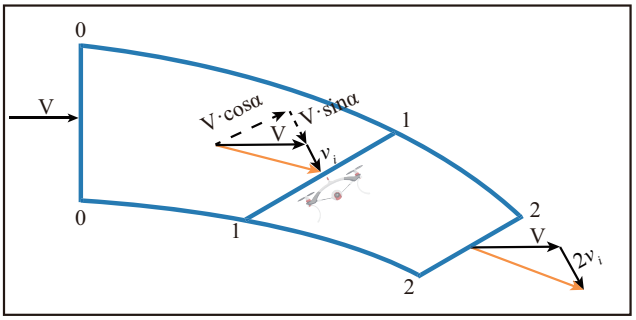

Figure 7. Illustration of control volume in forward flight. The air velocity V is approaching the rotor disc with an angle of α. According to (4), the induced velocity v_i at Section 1 will be double in Section 2.

Therefore, the Formula (18) can be approximated as

$$T \approx 2\rho A v_i\sqrt{V^2 + v_i^2}. \tag{19}$$

The above formula can be rewritten as

$$v_i^4 + V^2 v_i^2 - v_0^2 = 0, \tag{20}$$

where v_0 denotes the induced velocity in hovering as defined in (7).

Therefore, the induced velocity v_i can be expressed as

$$v_i = v_0\left(\sqrt{\frac{V^4}{4v_0^4} + 1} - \frac{V^2}{2v_0}\right)^{\frac{1}{2}}. \tag{21}$$

The induced power can be expressed as

$$P_{i,h} = Tv_i = \frac{T^{\frac{3}{2}}}{\sqrt{2\rho A}}\left(\sqrt{\frac{V^4}{4v_0^4} + 1} - \frac{V^2}{2v_0^2}\right)^{\frac{1}{2}}. \tag{22}$$

In forward flight, the parasite power is necessary to overcome the fuselage drag, which is described by ([37], Equation (4.5)) as

$$P_{par} = DV = \frac{1}{2}\rho S_{FP} V^3, \tag{23}$$

where S_{FP} is the equivalent flat plate area of the UAV.

Hence, the required power in forward flight is represented as

$$\begin{aligned} P_h &= P_{pro,h} + P_{i,h} + P_{par} \\ &= \frac{\sigma}{8}\rho A \bar{C}_D \Omega^3 R^3 (1 + 3\mu^2) \\ &+ \frac{\kappa W^{\frac{3}{2}}}{\sqrt{2\rho A}} \left(\sqrt{\frac{V^4}{4v_0^4} + 1} - \frac{V^2}{2v_0} \right)^{\frac{1}{2}} \\ &+ \frac{1}{2}\rho S_{FP} V^3. \end{aligned} \tag{24}$$

similarly, κ corrects the deviation between theoretical and practical values of induced power. And, T is approximated as W. Figure 8 shows the three power components and the total required power in horizontal flight versus the constant velocity of the UAV. It can be seen that the power consumed by the UAV decreases first, affected by the translational lift, and then increases, affected by fuselage drag [39]. Researchers have conducted experiments to verify the correctness of the energy model in straight-and-level flight. They applied two fitting techniques, namely model-based and model-free, to fit the measurement data and observed that the two fittings match quite well with each other [37].

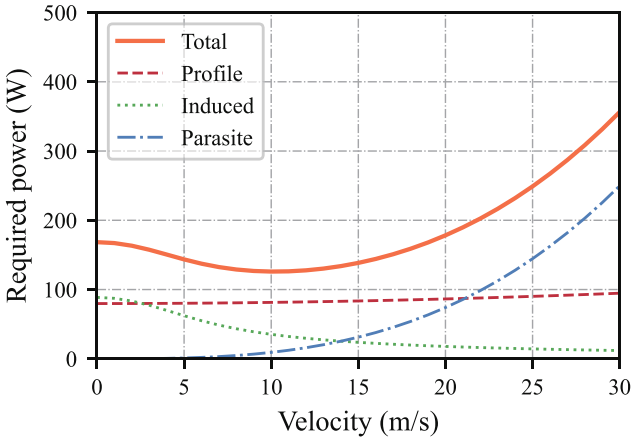

Figure 8. Profile, induced, and parasite power for horizontal flight.

2.2. Trajectory Planning Model

A whole UAV trajectory might consist of numerous segments to account for obstacle avoidance.

$$\mathcal{J} = \begin{cases} J_1 & t_0 \le T_1 \le t_1, \\ \vdots & \\ J_i & t_{i-1} \le T_i \le t_i, \\ \vdots & \\ J_M & t_{M-1} \le T_M \le t_M, \end{cases} \tag{25}$$

where $i = 1, \ldots, M$ indicates the ith segment.

The energy usage in each segment is calculated by dividing the ith flight segment into N slots with $\Delta t_{i,j}$, which is represented as

$$T_i = \sum_{j=1}^{N} \Delta t_{i,j}, \; i = 0, 1, \cdots, M, \tag{26}$$

where T_i is the duration of the ith segment and j denotes the index of the time slots within each segment.

We assume that the UAV is in a quasi-static equilibrium condition in each time slot. This means that the UAV moves smoothly with a small acceleration, and that the flight speed is constant throughout each time slot. We denote $\mathbf{v}_{i,j} = \left[v_{i,j}^x, v_{i,j}^y, v_{i,j}^z\right]$ as the velocity and $\mathbf{s}_{i,j} = \left[s_{i,j}^x, s_{i,j}^y, s_{i,j}^z\right]$ as the position during the ith segment and jth time slot, where v^x, v^y, and v^z are the velocity components of $\mathbf{v}$ and s^x, s^y, and s^z are the position components of $\mathbf{s}$ in 3D Cartesian coordinates. Each segment has N slots and $N+1$ velocity and position points. Each velocity point should be constrained by the velocity limit V_{max}, which can be expressed as

$$-V_{max} \leq \mathbf{v}_{i,j} \leq V_{max}. \tag{27}$$

Formula (28) ensures that the acceleration and deceleration stay within the permited limit.

$$-A_{max,d} \leq \frac{\|\mathbf{v}_{i,j} - \mathbf{v}_{i,j-1}\|}{\Delta t_{i,j}} \leq A_{max,a}. \tag{28}$$

The velocity of each slot's endpoint is used to determine the displacement of each slot, and the position can be calculated by

$$\mathbf{s}_{i,j} = \mathbf{s}_{i,j-1} + \mathbf{v}_{i,j}\Delta t_{i,j}. \tag{29}$$

We used a method similar to that in [16] to build a series of obstacle-free flying blocks where the trajectory must stay.

$$B_{i,min} \leq \|\mathbf{s}_{i,j}\| \leq B_{i,max}, \tag{30}$$

where $B_{i,min}$ and $B_{i,max}$ are the lower and upper boundaries of the corresponding ith block.

To maintain trajectory continuity, it is necessary for the final velocity and position of the $(i-1)$th segment to match the initial velocity and position of the ith segment.

$$\mathbf{v}_{i-1,N} = \mathbf{v}_{i,0}, \tag{31}$$

$$\mathbf{s}_{i-1,N-1} = \mathbf{s}_{i,0}. \tag{32}$$

The power rate equations derived in Section 2.1 are used to compute the power of each slot throughout the delivery mission.

$$p_{i,j} = P_h(\|v_{i,j}^x, v_{i,j}^y\|) + P_v(v_{i,j}^z), \tag{33}$$

where $\|v_{i,j}^x, v_{i,j}^y\|$ represents the horizontal velocity of the UAV.

The following formula can be used to calculate the energy consumption of each time slot.

$$e_{i,j} = p_{i,j}\Delta t_{i,j}. \tag{34}$$

The objective function is minimizing the total energy consumption of the whole flight.

$$\begin{aligned} &\min \sum_{i=1}^{M}\sum_{j=1}^{N} e_{i,j}, \\ &\text{s.t. } (25)\text{–}(34). \end{aligned} \tag{35}$$

The model described above is formulated as a quadratically constrained program (QCP), which can be efficiently solved using existing convex optimization solvers such as Gurobi and Cplex. Numerical experiments in Section 3 verify the model's effectiveness.

3. Experiment and Discussion

3.1. Numerical Experiment

In this section, numerical experiments were carried out to validate the effectiveness of the proposed energy-efficient trajectory generation approach for UAVs.

The least squares method (LSM) was used to fit vertical and horizontal power curves, and the results are shown in Figure 9. The original power data and the corresponding fitting power curves, with their coefficients listed in Table 2, exhibit a high degree of similarity. The fitted curves closely align with the original data, as indicated by the high R-square values of 0.8414 and 0.9748 for the two fitting results, respectively. To avoid introducing absolute values because they lead to the nonconvexity of the model, we fitted the data as symmetric quadratic curves so that the positive and negative speeds could correspond to positive power.

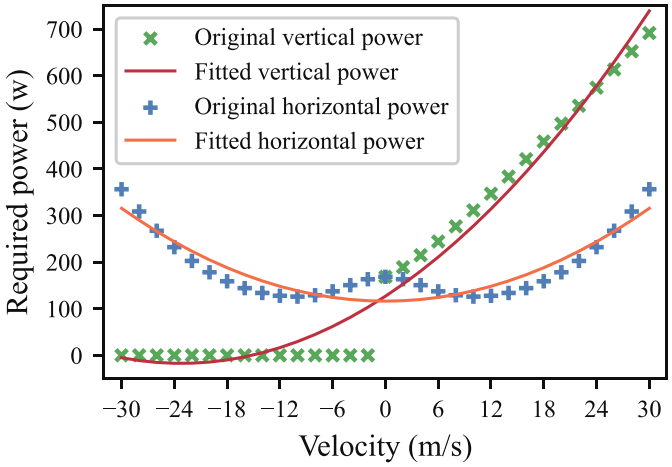

Figure 9. The original power data and the corresponding fitted curve in vertical and horizontal flight.

Table 2. Modelling parameters.

Parameter	Value	Parameter	Value
$c_{0,h}$ (Nm/s)	116.25	W (N)	20
$c_{1,h}$ (N)	0	V_{max} (m/s)	30
$c_{2,h}$ (N/(m/s))	0.22	$A_{max,d}$ (m/s^2)	2
$c_{0,v}$ (Nm/s)	123.20	$A_{max,a}$ (m/s^2)	2
$c_{1,v}$ (N)	12.45	M	6
$c_{2,v}$ (N/(m/s))	0.28	N	100

Figure 10 is a schematic diagram to illustrate the result of the proposed method, which includes the following three steps.

1. Apply the A* algorithm to search for a feasible path composed of discrete waypoints.
2. Choose the waypoints to expand and generate a series of connected obstacle-free blocks.
3. Allocate a suitable duration to each segment and solve the quadratically constrained program problem subjected to (25)–(34) with an objective function (35) to generate the minimum amount of energy consumption and the obstacle avoidance trajectory.

To validate the feasibility of the method proposed in this paper, we construct a static environment containing several obstacles. In the simulated scenario, we manually set the initial point at $(0, 0, 0)$ and the task's destination at $(4000, 500, 60)$. The total flight time of the whole mission is set as 350 s. We aim to generate an energy-efficient trajectory from

the start to the target location without collisions. Firstly, we applied the A* algorithm to generate the initial path, composed of multiple waypoints. Subsequently, we select some waypoints to expand, resulting in obstacle-free flight blocks. We implemented a blocks fusion algorithm, so the number of selected waypoints is not particularly strict. From our experience, selecting 10–20 waypoints is considered sufficient for algorithnm implementation. It is essential to confine the entire trajectory of the UAV within these flight blocks. Finally, we employed the proposed algorithm to obtain an obstacle-avoidance trajectory with optimal energy consumption. Numerical experiments were executed using a computer setup comprising an *Intel i9* CPU with a clock frequency of 3.1 GHz and 16 GB RAM. GUROBI 12.0.0 was used to address the problem subjected to (25)–(34) to minimize the sum of $e_{i,j}$. The modeling parameters are listed in Table 2. We set the maximum acceleration/deceleration to $2\,m/s^2$ according to [19], while the remaining parameters of the UAV are listed in Table 1.

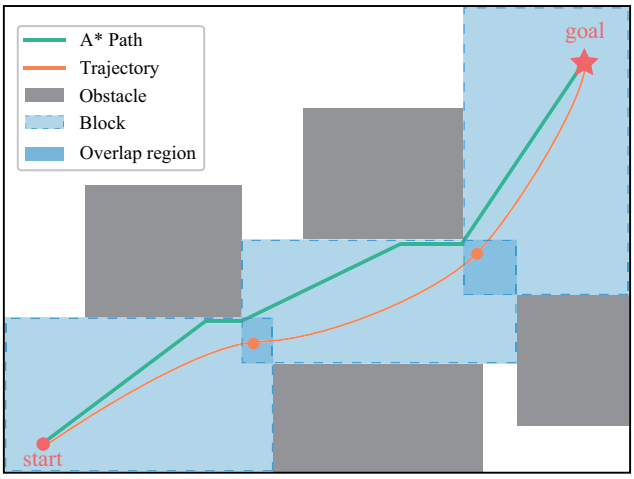

Figure 10. Schematic demonstration of the result using the proposed method. The gray boxes in the diagram represent obstacles. The green line demonstrates the A* path. Light blue boxes represent flight blocks. The darker region indicates the overlapping area of adjacent blocks. The orange line represents the optimized trajectory. The orange circle represents the intersection of the two trajectory segments.

Based on the number of flight blocks, the trajectory is divided into six segments. To allocate time for each segment, we employ the following time allocation strategy outlined in Algorithm 1. First, distribute the given mission time equally to each block and solve the model once. Second, calculate the distance of each trajectory segment. Third, reallocate time to blocks based on the proportion of the distance of each segment to the total distance. Eventually, solve the model again with the reallocated time. After applying the above time allocation strategy, the mission time for each segment is 71 s, 77 s, 47 s, 54 s, 45 s, and 56 s.

Four energy-efficient trajectories for different obstacle environments are depicted in Figure 11. For a better presentation, obstacles have been removed, leaving only flight blocks and trajectories. Figure 11 demonstrates that the UAV successfully arrives at the target location from the initial location while being constrained within the flight blocks. The optimal speed in horizontal and vertical directions of the trajectory in Figure 11a with the corresponding power are shown in Figure 12a and Figure 12b, respectively. The vertical and horizontal velocity does not exceed the maximum. The changing power trend is consistent with that of speed because the fitted power equation gradually rises with the increase in speed. The speed and power characteristics of the other trajectories exhibit similar trends and are therefore not elaborated further. In addition, when $V_c < 0$, the vertical power is not equal to 0 due to the curve fitting error, indicating that the power evaluation of this

model is conservative. The total energy consumption following the optimal trajectory is 103.29 kJ, which demonstrates the effectiveness and efficiency of the proposed method.

The number of trajectory points, N, is 100, the computational time is 0.12 s. For N = 1000, the computational time increases to 3.48 s, which is 29 times that of 0.12 s. When N = 10,000, the computational time reaches 74.27 s, approximately 21 times that of 3.48 s. As the number of trajectory points increases, the growth rate of computation time remains relatively slow, indicating that the computational complexity of the method is low.

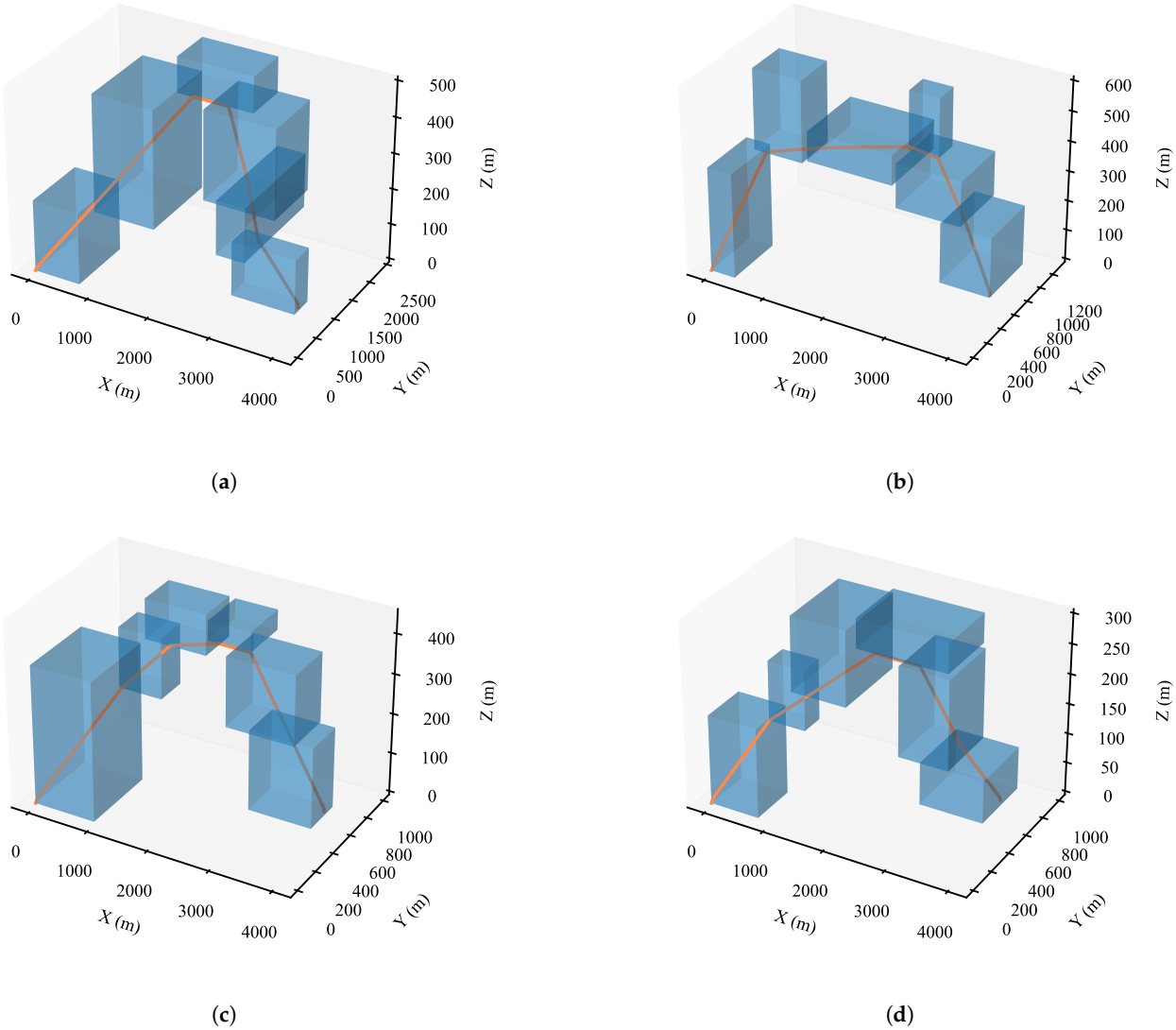

Figure 11. UAV trajectories in different 3D structured static environments. The orange curves demonstrate the trajectory generated by our method. Light blue boxes represent obstacle-free flight blocks. Subfigure (**a**–**d**) show flight trajectories of UAV under different static obstacle environments.

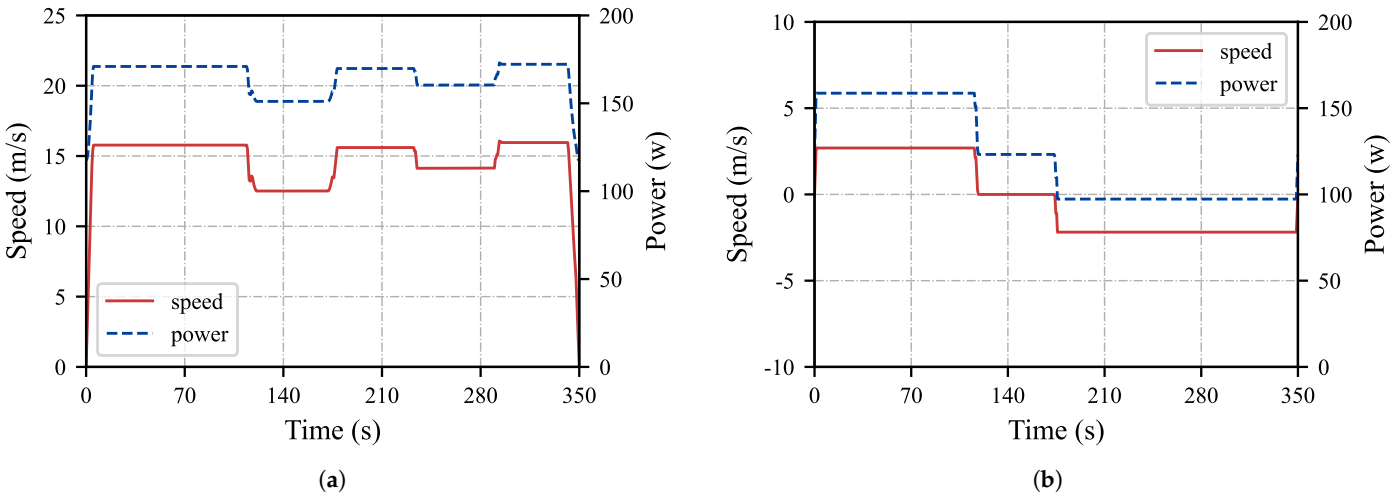

Figure 12. Energy-efficient speed profile and corresponding power in the (**a**) horizontal and (**b**) vertical directions.

Algorithm 1 Reallocation of mission time

Input: mission time T_t and system parameter settings.

Initialization: the set of waypoints $P \leftarrow \{\mathbf{0}\}$, the set of distance of waypoints $D \leftarrow \{\}$, the set of reallocation time for each block $T \leftarrow \{\}$, the total distance of waypoints $TD \leftarrow 0$.
Solve model (35) with T_t distributed equally to each block.
for $i = 1; i <= M; i++$ **do**
    $P \leftarrow P \cup J_{i,N}$;
end for
for $i = 1; i <= M; i++$ **do**
    $d_i = ||P_i, P_{i-1}||$;
    $D \leftarrow D \cup d_i$;
    $TD \leftarrow TD + d_i$;
end for
for $i = 1; i <= M; i++$ **do**
    $t_i = D_i / TD * T_t$;
    $T \leftarrow T \cup t_i$;
end for

Output: T.

3.2. Impact of Different Mission Times and Payloads

In this subsection, the influence of time and payload weight on the speed trajectory and energy consumption is investigated. We conduct an experiment using five different times for the above scenario, including 300 s, 325 s, 350 s, 375 s, and 400 s. Additionally, to explore the impact of different payload weights, we consider scenarios with payload weights with 0 N, 5 N, and 10 N for each mission time.

The velocity curves with different times are depicted in Figure 13. It can be seen from the figure that the velocity steadily decreases with increasing time, which is consistent with our expectations. The energy consumption with different times and payload weights is indicated in Figure 14. The line chart demonstrates that as time grows, energy consumption increases gradually. This can be attributed to the fact that although the corresponding power decreases as the speed reduces, the increase in time is higher than the loss of power, resulting in higher energy consumption. Moreover, it can be seen from Figure 14 that the energy consumption of UAVs gradually increases with the payload weight under scenarios within the specified time. This makes sense because the Formulas (11) and (24) indicate a positive correlation between power and UAV weight.

Furthermore, the energy consumptions required to complete the tasks when the UAV's speed was set to the average speed of the optimized trajectory without load have been evaluated, as indicated by the yellow line in Figure 14. It is evident that the UAV's energy consumption after trajectory velocity optimization is significantly lower compared to the non-optimized scenario. However, as the duration of the mission increases, the energy consumption in both conditions converges. This convergence occurs because, over extended mission times, the UAV's speed decreases and stabilizes. Consequently, the shorter the mission duration, the greater the energy savings achieved by the optimized trajectory before the UAV reaches its maximum speed limit.

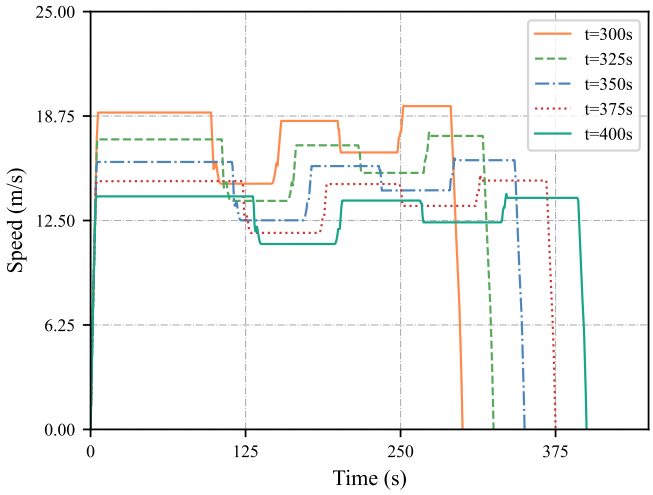

Figure 13. Resultant speed curve at five different times.

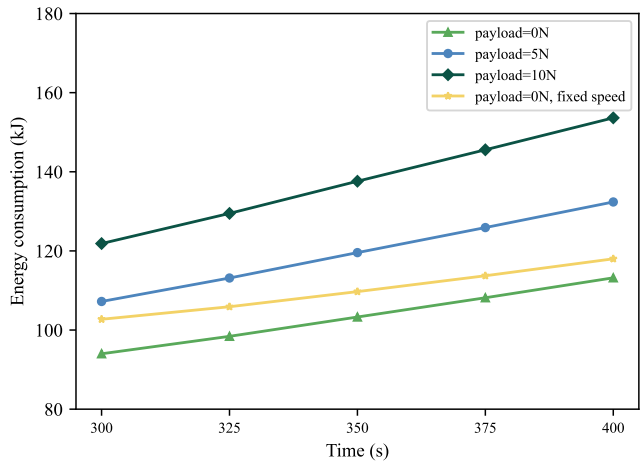

Figure 14. Energy consumption at five different times and three different payloads.

3.3. Mission Time Optimization

This subsection aimed at optimizing the logistics task duration. As discussed in Section 3.2, the energy consumption decreases as the mission time decreases. Consequently, under the condition of ensuring the successful completion of the mission, optimizing the mission time can lead to a reduction in energy consumption. Considering the monotonic relationship between energy consumption and time, we present the procedure for obtaining the minimum mission time for the UAV as Algorithm 2 using the binary searching method. The environment and parameter settings, trajectory planning, and time allocation strategy are the same as those in Section 3.1. The algorithm is used to search for the minimum time to complete the mission for the trajectory in Figure 11a in $[0, 500]$ s. The results show that

the minimum mission completion time is 210 s. The corresponding energy consumption is 81.96 kJ, which is less than that of the case in Section 3.1 with a mission time of 350 s.

Algorithm 2 Mission time optimization

Input: Mission time range $[T_{min}, T_{max}]$, environment and parameter settings.
1: Initialization: $l \leftarrow T_{min}, r \leftarrow T_{max}$.
2: **while** $l < r$ **do**
3: $mid \leftarrow \lfloor (l + r)/2 \rfloor$;
4: **if** Model (35) can be solved with reallocated time determined by mid. **then**
5: $r \leftarrow mid$;
6: **else**
7: $l \leftarrow mid + 1$;
8: **end if**
9: **end while**
Output: Minimum mission complete time.

4. Conclusions and Future Work

In this paper, we derived an energy consumption model for multi-rotor UAVs. With this model, we introduced an energy-efficient trajectory planning problem for multi-rotor UAVs, formulated as a quadratically constrained program problem, and efficiently addressed it. We employed the A* algorithm as the front-end path-searching approach to generate a safe flight corridor. The trajectory was divided into several segments according to the number of generated obstacle-free blocks. The mission time was allocated to each block according to the partition of each trajectory segment's distance to the whole trajectory. Finally, a time discretization approach was adopted to optimize the energy usage of the entire trajectory.

Numerical experiments were carried out to validate the effectiveness of the proposed method. The effect of different mission times and payload weights on energy consumption was investigated. The results demonstrated that the UAV consumes more energy as the mission time and payload weight increase. Furthermore, a binary search method was used to find the optimal mission time iteratively. Further research will be conducted to improve the time allocation of each trajectory segment to balance the mission time and energy consumption. Moreover, the application in a complex dynamic environment is also worth exploring.

Moreover, the proposed framework's potential for application in complex dynamic environments warrants further investigation. In dynamic scenarios, where obstacles and environmental conditions may change over time, the current use of the A* algorithm for front-end path searching may not be suitable. Advanced algorithms, such as D* or its dynamic variants, could provide more adaptive and efficient solutions. Additionally, the integration of artificial intelligence techniques, including reinforcement learning and deep learning, offers a promising avenue to enhance the framework's adaptability and decision-making capabilities in highly dynamic and uncertain environments.

Further applications in real-world dynamic scenarios, such as urban environments with moving obstacles or collaborative multi-UAV missions, could also be explored. The framework could be extended to include predictive models for obstacle movement, real-time trajectory adjustment, and multi-agent coordination, ensuring both energy efficiency and mission success under varying operational conditions. These advancements would significantly enhance the framework's robustness and broaden its applicability to more complex and challenging UAV operations.

Author Contributions: Conceptualization, K.W.; data curation, J.L.; formal analysis, J.L.; funding acquisition, S.L.; investigation, C.W.; methodology, K.W.; project administration, S.L.; resources, Z.L.; software, K.W.; supervision, S.L.; validation, K.W. and J.L.; visualization, B.L.; writing—original draft, K.W.; writing—review and editing, S.L. and J.L. All authors have read and agreed to the published version of the manuscript.

Funding: This work was supported in part by the National Natural Science Foundation of China (Grant No. 52472343, 52302380), in part by the National Science Foundation of Guangdong Province, China (Grant No. 2023A1515012949), in part by the Featured Innovation Project of the Department of Education of Guangdong Province under Grant 2021KTSCX001, and in part by the Fujian Zhongli Technology Co., Ltd. (Contract No. x2znD9211960).

Institutional Review Board Statement: Not applicable.

Informed Consent Statement: Not applicable.

Data Availability Statement: The original contributions presented in this study are included in the article material. Further inquiries can be directed to the corresponding author.

Acknowledgments: We are grateful to our colleagues for their valuable feedback and constructive discussions that enriched this study.

Conflicts of Interest: Author Zenghao Lu was employed by Fujian Zhongli Technology Co. The remaining authors declare that the research was conducted in the absence of any commercial or financial relationships that could be construed as a potential conflict of interest. The authors declare that this study received funding from Fujian Zhongli Technology Co. The funder was not involved in the study design, collection, analysis, interpretation of data, the writing of this article or the decision to submit it for publication.

References

1. D'Andrea, R. Guest Editorial Can Drones Deliver? *IEEE Trans. Autom. Sci. Eng.* **2014**, *11*, 647–648. [CrossRef]
2. Ma, F.; Xu, Z.; Xiong, F. Research on Route Planning of Plant Protection UAV Based on Area Modular Division. In Proceedings of the 11th International Conference on Intelligent Human-Machine Systems and Cybernetics (IHMSC), Hangzhou, China, 24–25 August 2019; pp. 101–104. [CrossRef]
3. Ma, T.; Li, B.Y.; Nie, G.F. An Energy Saving Routing Strategy with Differentiated Service Provide Ability for UAV Assisted Disaster Rescue. In Proceedings of the 7th International Conference on Computer and Communications (ICCC), Chengdu, China, 10–13 December 2021; pp. 64–69. [CrossRef]
4. Li, Y.; Liu, M.; Jiang, D.D. Application of unmanned aerial vehicles in logistics: A literature review. *Sustainability* **2022**, *14*, 14473. [CrossRef]
5. Dorling, K.; Heinrichs, J.; Messier, G.G.; Magierowski, S. Vehicle Routing Problems for Drone Delivery. *IEEE Trans. Syst. Man Cybern. Syst.* **2017**, *47*, 70–85. [CrossRef]
6. Zeng, Y.; Zhang, R. Energy-Efficient UAV Communication With Trajectory Optimization. *IEEE Trans. Wirel. Commun.* **2017**, *16*, 3747–3760. [CrossRef]
7. Quan, L.; Han, L.X.; Zhou, B.Y.; Shen, S.J.; Gao, F. Survey of UAV motion planning. *IET Cyber-Syst. Robot.* **2020**, *2*, 14–21. [CrossRef]
8. LaValle, S.M. *Rapidly-Exploring Random Trees: A New Tool for Path Planning*; The Annual Research Report; The MIT Press: Cambridge, MA, USA, 1 January 1998. Available online: https://api.semanticscholar.org/CorpusID:14744621 (accessed on 13 December 2024).
9. Likhachev, M.; Gordon, G.; Thrun, S. ARA*: Anytime A* with Provable Bounds on Sub-Optimality. In Proceedings of the 16th International Conference on Neural Information Processing Systems, Cambridge, MA, USA, 9–11 December 2003; pp. 767–774. [CrossRef]
10. Siméon, T.; Laumond, J.-P.; Nissoux, C. Visibility-based probabilistic roadmaps for motion planning. *Adv. Robot.* **2000**, *14*, 477–493. [CrossRef]
11. Lavalle, S.; Kuffner, J. Rapidly-Exploring Random Trees: Progress and Prospects. *Algorithmic and Computational Robotics: New Directions*; CRC Press: Boca Raton, FL, USA, 1 January 2000. Available online: https://api.semanticscholar.org/CorpusID:264621287 (accessed on 13 December 2024).

12. Guo, Y.; Liu, X.; Jia, Q. HPO-RRT*: A sampling-based algorithm for UAV real-time path planning in a dynamic environment. *Complex Intell. Syst.* **2023**, *9*, 7133–7153. [CrossRef]
13. Fan, J.M.; Chen, X.; Liang, X. UAV trajectory planning based on bi-directional APF-RRT* algorithm with goal-biased. *Expert Syst. Appl.* **2023**, *213*, 119137. [CrossRef]
14. He, Y.; Hou, T.; Wang, M. A new method for unmanned aerial vehicle path planning in complex environments. *Sci. Rep.* **2024**, *14*, 9257. [CrossRef]
15. Huang, Y.L.; Guo, S.J. Path planning of mobile robots based on improved A* algorithm. In Proceedings of the 2022 Asia Conference on Advanced Robotics, Automation, and Control Engineering (ARACE), Qingdao, China, 26–28 August 2022; pp. 133–137. [CrossRef]
16. Gao, F.; Wu, W.; Lin, Y.; Shen, S.J. Online Safe Trajectory Generation For Quadrotors Using Fast Marching Method and Bernstein Basis Polynomial. In Proceedings of the IEEE International Conference on Robotics and Automation (ICRA), Brisbane, QLD, Australia, 21–25 May 2018; pp. 344–351. [CrossRef]
17. Mellinger, D.; Kumar, V. Minimum snap trajectory generation and control for quadrotors. In Proceedings of the IEEE International Conference on Robotics and Automation, Shanghai, China, 9–13 May 2011; pp. 2520–2525. [CrossRef]
18. Richter, C.; Bry, A.; Roy, N. Polynomial Trajectory Planning for Aggressive Quadrotor Flight in Dense Indoor Environments. In *Robotics Research, Proceedings of the 16th International Symposium ISRR, Singapore, 16–19 December 2013*; Inaba, M., Corke, P., Eds.; Springer Publishing Company: Cham, Switzerland, 2016; pp. 649–666. [CrossRef]
19. Chen, J.; Su, K.Y.; Shen, S.J. Real-Time Safe Trajectory Generation for Quadrotor Flight in Cluttered Environments. In Proceedings of the IEEE International Conference on Robotics and Biomimetics, Zhuhai, China, 6–9 December 2015; pp. 1678–1685. [CrossRef]
20. Chen, J.; Liu, T.B.; Shen, S.J. Online Generation of Collision-Free Trajectories for Quadrotor Flight in Unknown Cluttered Environments. In Proceedings of the IEEE International Conference on Robotics and Automation, Stockholm, Sweden, 16–21 May 2016; pp. 1476–1483. [CrossRef]
21. Gao, F.; Shen, S.J. Online quadrotor trajectory generation and autonomous navigation on point clouds. In Proceedings of the IEEE International Symposium on Safety, Security, and Rescue Robotics, Lausanne, Switzerland, 23–27 October 2016; pp. 139–146. [CrossRef]
22. Tang, L.B.; Wang, H.S.; Liu, Z.; Wang, Y. A real-time quadrotor trajectory planning framework based on B-spline and nonuniform kinodynamic search. *J. Field Robot.* **2020**, *38*, 452–475. [CrossRef]
23. Foehn, P.; Romero, A.; Scaramuzza, D. Time-optimal planning for quadrotor waypoint flight. *Sci. Robot.* **2021**, *6*, eabh1221. [CrossRef] [PubMed]
24. Zeng, Y.; Xu, J.; Zhang, R. Energy Minimization for Wireless Communication With Rotary-Wing UAV. *IEEE Trans. Wirel. Commun.* **2019**, *18*, 2329–2345. [CrossRef]
25. Raj, R.; Murray, C. The multiple flying sidekicks traveling salesman problem with variable drone speeds. *Transp. Res. Part C Emerg. Technol.* **2020**, *120*, 102813. [CrossRef]
26. Du, P.; He, X.; Cao, H.; Garg, S.; Kaddoum, G.; Hassan, M.M. AI-based energy-efficient path planning of multiple logistics UAVs in intelligent transportation systems. *Comput. Commun.* **2023**, *207*, 46–55. [CrossRef]
27. Zhang, J.; Campbell, J.F.; Sweeney, D.C., II; Hupman, A.C. Energy consumption models for delivery drones: A comparison and assessment. *Transp. Res. Part D Transp. Environ.* **2021**, *90*, 102668. [CrossRef]
28. Cheng, C.; Adulyasak, Y.; Rousseau, L.-M. Drone routing with energy function: Formulation and exact algorithm. *Transp. Res. Part B* **2020**, *139*, 365–387. [CrossRef]
29. Du, P.; Shi, Y.; Cao, H.; Garg, S.; Alrashoud, M.; Shukla, P.K. AI-Enabled Trajectory Optimization of Logistics UAVs With Wind Impacts in Smart Cities. *IEEE Trans. Consum. Electron.* **2024**, *70*, 3885–3897. [CrossRef]
30. Rinaldi, M.; Primatesta, S.; Guglieri, G.; Rizzo, A. Multi-Auctioneer Market-based Task Scheduling for Persistent Drone Delivery. In Proceedings of the 2023 International Conference on Unmanned Aircraft Systems (ICUAS), Warsaw, Poland, 6–9 June 2023; pp. 790–797. [CrossRef]
31. Thibbotuwawa, A. Energy Consumption in Unmanned Aerial Vehicles: A Review of Energy Consumption Models and Their Relation to the UAV Routing. In Proceedings of the Information Systems Architecture and Technology: Proceedings of the 39th International Conference on Information Systems Architecture and Technology—ISAT 2018, Nysa, Poland, 16–18 September 2018; Springer: Cham, Switzerland, 2018; pp. 173–184. [CrossRef]
32. Stolaroff, J.K.; Samaras, C.; Mitchell, A.S.; Ceperley, D.; O'Neill, E.R.; Lubers, A. Energy use and life cycle greenhouse gas emissions of drones for commercial package delivery. *Nat. Commun.* **2018**, *9*, 409. [CrossRef] [PubMed]
33. Stolaroff, J.K.; Samaras, C.; Mitchell, A.S.; Ceperley, D.; O'Neill, E.R.; Lubers, A. A power consumption model for multi-rotor small unmanned aircraft systems. In Proceedings of the 2017 International Conference on Unmanned Aircraft Systems (ICUAS), Miami, FL, USA, 13–16 June 2017; pp. 310–315. [CrossRef]
34. Yang, Z.H.; Xu, W.; Shikh-Bahaei, M. Energy Efficient UAV Communication With Energy Harvesting. *IEEE Trans. Veh. Technol.* **2020**, *69*, 1913–1927. [CrossRef]

35. Yan, H.; Chen, Y.F.; Yang, S.-H. New Energy Consumption Model for Rotary-Wing UAV Propulsion. *IEEE Wirel. Commun. Lett.* **2021**, *10*, 2009–2012. [CrossRef]
36. Dai, X.H.; Duo, B.; Yuan, X.J.; Tang, W.B. Energy-Efficient UAV Communications: A Generalised Propulsion Energy Consumption Model. *IEEE Wirel. Commun. Lett.* **2022**, *10*, 2150–2154. [CrossRef]
37. Gao, N.; Zeng, Y.; Wang, J.; Wu, D.; Zhang, C.Y.; Song, Q.H.; Qian, J.; Jin, S. Energy model for UAV communications: Experimental validation and model generalization. *China Commun.* **2021**, *18*, 253–264. [CrossRef]
38. Chan, C.W.; Kam, T.Y. A procedure for power consumption estimation of multi-rotor unmanned aerial vehicle. *J. Phys. Conf. Ser.* **2020**, *1509*, 012015. [CrossRef]
39. Bramwell, A.; Done, G.; Balmford, D. *Bramwell's Helicopter Dynamics*, 2nd ed.; Butterworth-Heinemann: Oxford, UK, 2000; pp. 33–114. [CrossRef]
40. Meng, A.Q.; Gao, X.Z.; Zhao, Y.; Yang, Z.X. Three-Dimensional Trajectory Optimization for Energy-Constrained UAV-Enabled IoT System in Probabilistic LoS Channel. *IEEE Internet Things J.* **2022**, *9*, 1109–1121. [CrossRef]